On the Modeling of Hydraulic Components in Rotorcraft Systems*

Olivier A. Bauchau and Haiying Liu
School of Aerospace Engineering,
Georgia Institute of Technology, Atlanta, GA, USA.

March 28, 2016

Abstract

A physics based methodology for modeling of hydraulic devices within multibody-based comprehensive models of rotorcraft systems is developed. The proposed models are developed in two stages. At first, models are developed for three basic hydraulic elements: the hydraulic chamber, the hydraulic orifice and the pressure relief valve. These models consist of nonlinear differential equations involving empirical parameters. Next, these basic elements are combined to yield device models for linear hydraulic actuators, simple hydraulic dampers, and hydraulic dampers with pressure relief valves. The proposed hydraulic device models are implemented in a multibody code and calibrated by comparing their predictions with test bench measurements for the UH-60 helicopter lead-lag damper. While predicted peak damping forces are found to be in good agreement with measurements, the model does not predict the entire time history of damper force to the same level of accuracy. The validated model of the UH-60 lead-lag damper model is coupled with a comprehensive model of the vehicle. Measured aerodynamic loads are applied to the blade and predicted damper forces are compared with experimental measurements. A marked improvement in the prediction is observed when using the proposed model rather than a linear approximation of the damper behavior.

1 Introduction

The behavior of hydraulic actuators and dampers can be modeled in several manners. In the first approach, very simple idealizations of hydraulic components are used. For instance, a hydraulic damper would be idealized as a dashpot: the force in the damper in proportional to the relative velocity of the piston. More often than not, actual damper will exhibit a nonlinear force-velocity relationship and a linear approximation is clearly too crude. The accuracy of the predictions might be improved if the damper is modeled as a nonlinear dashpot; this approach is widely used in industry. In that case, the nonlinear characteristics of the device are identified by a number of bench experiments, typically involving harmonic excitations of the device at various frequencies and amplitudes. The main drawback of this approach is that physical characteristics identified under harmonic excitation might not yield good results when the device is subjected to arbitrary excitation in time.

In the second approach, the hydrodynamic behavior of the device is linearized to obtain one or more ordinary differential equations relating control inputs to the forces generated by the device;

Journal of the American Helicopter Society, **51**(2), pp 175 – 184, 2006

typical equations are given in text books such as those of Viersma [1] or Canon [2]. While this approach is physics based and captures some basic aspects of hydraulic devices, the linearization process is clearly too restrictive. In fact, rotorcraft lead-lag dampers are often purposely designed to behave in a nonlinear manner. Indeed, a linear device would generate high damping forces under high stroking rates; these high forces must be reacted at the hub and at the root of the blade, creating high stresses and decreasing fatigue life. A possible remedy to this situation is to use pressure relief valves that act as force limiters, implying a nonlinearity essential to the design and behavior of the device.

In the last approach, a physics based, fully nonlinear representation of hydraulic devices is implemented. This enables the determination of the complex interaction phenomena between the structural and actuator dynamics: pressure levels in the hydraulic chambers are now coupled with the dynamic response of the system. This paper describes such an approach in detail, and its predictions are validated against bench test measurements and flight test data for Sikorsky's UH-60 aircraft.

The modeling of hydraulic devices has been the subject of detailed studies. Welsh [3] proposed a detailed model for predicting the dynamic response of helicopter air-oil landing gear that included several degrees of freedom representing the tire, floating piston, orifice piston, and simple fluid and adiabatic gas models. In a later effort [4], the same author addressed the problem of modeling the lubrication system of a helicopter using a similar approach. In both cases, detailed models of hydraulic systems were developed, but not coupled with the dynamic response of the vehicle.

A variety of hydraulic devices are used in the rotorcraft industry: hydraulic actuators are crucial components of many main rotor control systems, hydraulic lead-lag dampers are used in many rotor designs, and landing gear often involve hydraulic or pneumatic elements. In the case of lead-lag dampers, the hydraulic device tightly interacts with rotor response; in fact, blade root edgewise moments depend to a large extent on damper response characteristics. To deal with this variety of devices, a modular approach is taken. At first, models are developed for three basic hydraulic elements: the hydraulic chamber, the hydraulic orifice, and the pressure relief valve. Models for entire hydraulic devices are then constructed by assembling the models of a number these hydraulic elements. In this work, models for hydraulic actuators, simple hydraulic dampers, and hydraulic dampers with pressure relief valves are discussed.

Once a model of the hydraulic device is in hand, it is to be coupled with a comprehensive rotorcraft simulation code. In this effort, hydraulic device models are coupled to a finite element based multibody formulation of a helicopter rotor system within a comprehensive analysis [5]. Within the framework of flexible mechanism analysis codes, the modeling of hydraulic devices has attracted limited attention; Cardona and Géradin [6] proposed models for a hydraulic jack and for the actuator of an aircraft retractable landing gear.

Conceptually, the coupling of a hydraulic device model with a comprehensive rotorcraft modeling code is straightforward. First, the hydraulic device model predicts the instantaneous force the device applies on the supporting structure. In turn, this force is applied to the dynamic model of the vehicle to predict displacements and velocities. Finally, these kinematic quantities change the stroke of the hydraulic device, and hence, its force output. In a finite element formulation, this is readily achieved by connecting the end points of the hydraulic device to two nodes of the finite element discretization.

The present paper has two main goals. First, a comprehensive modeling approach will be presented for hydraulic devices, such as hydraulic actuators and dampers. Second, these models will be coupled to a comprehensive rotorcraft model using a finite element based multibody formulation. The paper is organized in the following manner. The first section presents models for the basic hydraulic elements, and the second section shows how these basic models can be combined to deal with various hydraulic devices. Next, issues associated with the coupling of hydraulic devices models with finite element based multibody formulations of rotorcraft dynamic simulation are discussed,

with special focus on the integration of the hydraulic equations. The modeling approach is then validated using a number of numerical examples. Finally, conclusions of this work are offered.

2 Basic Hydraulic Elements

Hydraulic devices can be seen as an assembly of simple hydraulic elements; in this work, three basic hydraulic elements will be presented: hydraulic chambers, orifices, and pressure relief valves. These basic elements are described in the following sections. Of course, a variety of other elements could be developed, such as hydraulic accumulators or check valves.

2.1 Hydraulic chamber

The hydraulic chamber, shown in fig. 1, is probably the most common hydraulic component. The chamber, of volume V and cross-sectional area A, is filled with a hydraulic fluid of bulk modulus B under pressure p. Often, due to the presence of a piston, the length of the chamber can vary. The change in length of the chamber, due to piston motion, is denoted d. Finally, hydraulic fluid can flow into the chamber; Q denotes the net volumetric flow rate into the chamber.

The evolution of the pressure in the chamber is governed by the following first order differential equation

$$\dot{p} = \frac{B}{V}\,(Q - A\,\lambda\dot{d}). \tag{1}$$

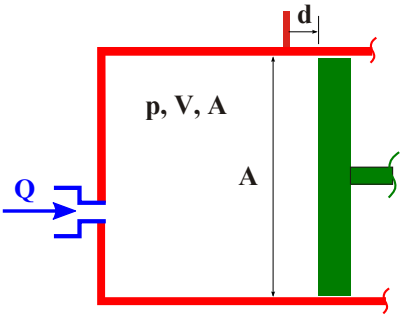

Figure 1: Configuration of a hydraulic chamber.

The factor λ is a configuration dependent parameter: if a positive value of d increases the volume of the chamber, $\lambda = +1$; $\lambda = -1$ in the opposite case. The instantaneous volume of the chamber is

$$V = V_0 + A\lambda d, \tag{2}$$

where V_0 is the initial volume of the hydraulic chamber. The bulk modulus of the hydraulic fluid is a function of the fluid pressure; an accurate approximation of this dependency is written as

$$B = \frac{1 + \alpha p + \beta p^2}{\alpha + 2\beta p}, \tag{3}$$

where α and β are physical constants for the hydraulic fluid [1].

2.2 Hydraulic orifice

The hydraulic orifice, shown in fig. 2, allows the flow of hydraulic fluid through an orifice of sectional area A_{orf}. The orifice is connected to two hydraulic chambers with pressures p_0 and p_1, respectively. A pressure differential, $\Delta p = p_0 - p_1$, will drive a volumetric flow rate, Q_{orf}, across the orifice; the positive direction of this flow rate is indicated on the figure. The magnitude of this volumetric flow rate is related to the pressure differential by the following equation

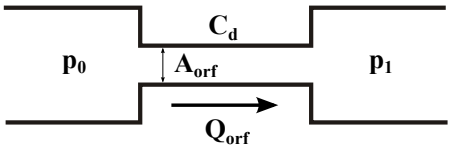

Figure 2: Configuration of a hydraulic orifice.

$$Q_{\text{orf}} = A_{\text{orf}} C_d \sqrt{\frac{2|\Delta p|}{\rho}}\,\frac{\Delta p}{|\Delta p|}, \tag{4}$$

where ρ denotes the mass density of the hydraulic fluid. For turbulent flow conditions, the theoretical value of the discharge coefficient, denoted C_d, is $C_d = 0.611$, seeViersma [1].

2.3 Pressure relief valve

The pressure relief valve, shown in fig. 3, is connected to two hydraulic chambers with pressures p_0 and p_1, respectively. It features a poppet of mass m connected to a spring of stiffness constant k and dashpot of viscous constant c; the spring is preloaded with a pre-load force. The equation of motion of the pressure relief valve is:

$$m\,\ddot{x} + c\dot{x} + kx = (p_0 A_0 - p_1 A_1) - F_p, \qquad (5)$$

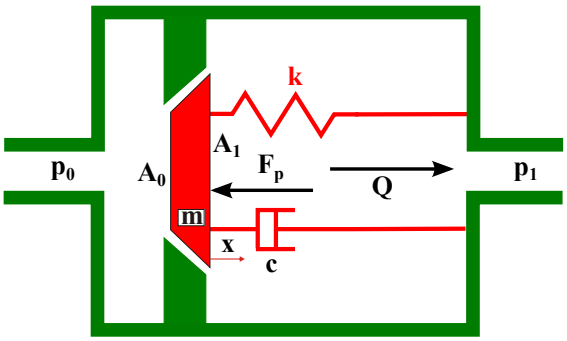

Figure 3: Configuration of a pressure relief valve.

where F_p is the pressure relief valve pre-load force. When the net force acting on the poppet is smaller than the pre-load force, *i.e.* when $p_0 A_0 - p_1 A_1 < F_p$, the valve remains closed, $x = \dot{x} = 0$. On the other hand, when the net force is large enough to overcome the pre-load force, the poppet opens and its motion is governed by eq. (5). Once the valve is open, fluid will flow through the valve at the following volumetric rate

$$Q_{\text{prvl}} = A_{\text{prvl}} C_d \sqrt{\frac{2|\Delta p|}{\rho}}\,\frac{\Delta p}{|\Delta p|}, \qquad (6)$$

where $\Delta p = p_0 - p_1$ is the pressure differential across the valve. The area A_{prvl} through which the fluid flows is a function of the valve opening

$$A_{\text{prvl}} = \begin{cases} ax + bx^2, & x > 0, \\ 0 & x \le 0, \end{cases} \qquad (7)$$

where a and b are coefficients defining the pressure relief valve sectional area.

The pressure relief valve acts as a pressure regulator: when the pressure differential across the valve becomes high enough, $p_0 A_0 > p_1 A_1 + F_p$, the valve open and the ensuing flow tends to equilibrate the pressures, at which point, the valve closes.

3 Hydraulic devices

The hydraulic elements described in the previous section can be combined to form practical hydraulic devices such as linear hydraulic actuators, simple dampers, or dampers with pressure relief valves that are described below. More complex devices could be modeled using the same technique.

3.1 Hydraulic linear actuator

The linear hydraulic actuator combines two hydraulic chambers, chamber 0 and chamber 1, and two orifices, orifice 0 and orifice 1, to form the configuration depicted in fig. 4. The hydraulic chamber 0 and chamber 1 are under pressures p_0 and p_1, respectively; note that the λ factors are $+1$ and -1 for the two chambers, respectively. The hydraulic orifice 0 and orifice 1 generate flow rates Q_0 and Q_1 into chambers 0 and 1, respectively. The two orifices have entrance pressures p_{E0} and p_{E1}, respectively. To increase the length of the actuator, control valves (not part of the present model)

will set the entrance pressure of orifice 0 to a high value, p_h, such that $p_{E0} = p_h$, while the entrance pressure of orifice 1 remains at a low value, p_s, such that $p_{E1} = p_s$; p_s denotes the hydraulic circuit background pressure. To decrease the length of the actuator, the control valves reverse the pressure level at the entrance to the two orifices.

The force generated by the actuator, denoted F^h, is

$$F^h = p_0 A_0 - p_1 A_1. \tag{8}$$

The governing equations for the linear hydraulic actuator include equations for the pressures p_0 and p_1 in the two chambers, eq. (1), and equations for the flow rates Q_0 and Q_1 through the orifices, eq. (4).

Most hydraulic actuators are also equipped with check valves that connect the hydraulic chambers to the circuit background pressure when the chamber pressure falls below the background pressure, in an effort to avoid cavitation in the chamber.

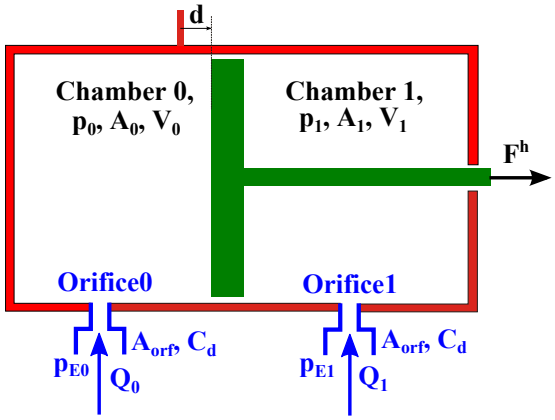

Figure 4: Configuration of the hydraulic actuator.

3.2 Simple hydraulic damper

The simple hydraulic damper combines two hydraulic chambers, chamber 0 and chamber 1, and one orifice connecting the two chambers to form the configuration depicted in fig. 5. The hydraulic chamber 0 and chamber 1 are under pressures p_0 and p_1, respectively; note that the λ factors are $+1$ and -1 for the two chambers, respectively. The hydraulic orifice generates a flow rate Q from chamber 0 into chamber 1. If the length of the damper increases (*i.e.* piston and rod move to the right in fig. 5, pressure p_1 increases whereas pressure p_0 decreases. This generates a pressure differential across the orifice and hence, a flow rate Q into chamber 0 that tends to equilibrate the pressures in the chambers. The force generated by the damper always opposes the motion and is therefore a damping force.

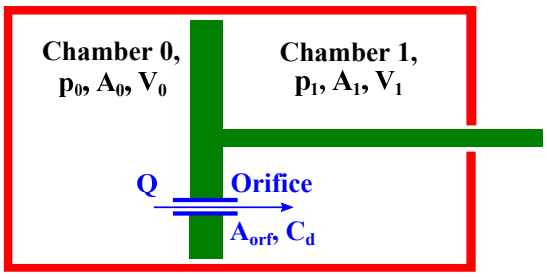

Figure 5: Configuration of the simple hydraulic damper.

The force generated by the damper is here again given by eq. (8). The governing equations for the simple hydraulic damper include equations for the pressure p_0 and p_1 in the two chambers, eq. (1), and one equation for the flow rate Q through the orifice, eq. (4).

3.3 Hydraulic damper with pressure relief valves

Rotorcraft hydraulic lead-lag dampers present a configuration similar to that of the simple damper described in the previous section. However, this simple design suffers an important drawback: under a high stroking rate, the pressure differential in the chambers can be rather high, and hence, high damping forces are generated. These high forces must be reacted at the hub and at the root of the blade, creating high stresses and decreasing fatigue life. To limit the forces in the hydraulic damper, two pressure relief valves are added to the configuration, as shown in fig. 6. The new design combines two hydraulic chambers, chamber 0 and chamber 1, one orifice connecting the two

chambers and two pressure relief valves, valve 0 and valve 1. The hydraulic chamber 0 and chamber 1 are under pressures p_0 and p_1, respectively; note that the λ factors are $+1$ and -1 for the two chambers, respectively. The hydraulic orifice generates a flow rate Q from chamber 0 into chamber 1. Finally, when open, the pressure relief valves regulate the pressures in chambers 0 and 1.

If the length of the damper increases, pressure p_1 increases whereas pressure p_0 decreases. This generates a pressure differential across the orifice and hence, a flow rate Q into chamber 0 that tends to equilibrate the pressures in the chambers. If the stroking rate is high, the pressure differential in the chambers will become high enough to open pressure relief valve 1, resulting in an additional flow rate Q_1 from chamber 1 into chamber 0. Given the sign of the pressure differential, valve 0 will remain closed. The opening of the valve and the ensuing flow controls the magnitude of the pressure differential, and hence of the damper force that is still given by eq. (8). The force generated by the damper always opposes the motion and is therefore a damping force. In practical designs, hydraulic dampers are also equipped with check valves, as discussed for actuators. The hydraulic chambers are connected to a plenum with oil at the circuit background pressure to prevent pressure drops in the chambers and subsequent cavitation.

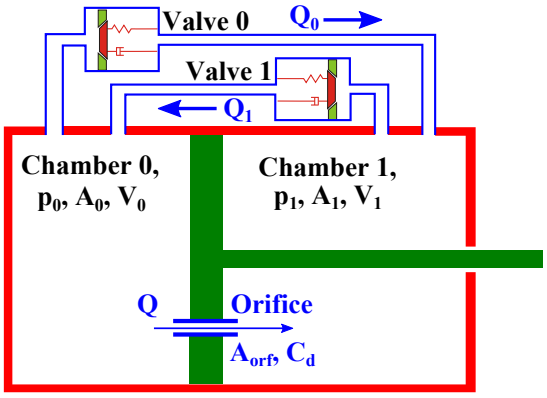

Figure 6: Configuration of the hydraulic damper with pressure relief valves.

The governing equations for the hydraulic damper with pressure relief valves include equations for the pressures p_0 and p_1 in the two chambers, eq. (1), one equation for the flow rate Q through the orifice, eq. (4), two equations of motion for the valve poppets, eq. (5), and two equations for the flow rates through the valves, eq. (6). The flow area of the valves is computed with the help of eq. (7).

4 Finite Element Implementation

The various hydraulic devices described in the previous section interact with the dynamics of the mechanical system they are connected to. For instance, a helicopter lead-lag damper interacts with rotor blade dynamics; this effect is particularly pronounced on the fundamental blade lead-lag mode. This section describes the coupling of the hydraulic device model with a structural dynamics model, within the framework of multibody system dynamics, see Ref. [5]. The following sections describe the coupling procedure in terms of the applied structural forces, their time discretization, and the time integration scheme for the equations governing the behavior of hydraulic devices.

4.1 Applied structural forces

In general, hydraulic devices generate hydraulic forces given by eq. (8) that are functions of the stroke d, through eq. (2) and stoke rate $\dot{d}$, through eq. (1). This stroking can be evaluated from the configuration of the device depicted in fig. 7. In the initial configuration, the end points of the device are at location $\underline{u}_0^k$ and $\underline{u}_0^\ell$, respectively, with respect to an inertial frame $\mathcal{I} = (\bar{\imath}_1, \bar{\imath}_2, \bar{\imath}_3)$. At those points, the device is connected to a dynamical system of arbitrary topology. In the deformed configuration, the displacements of the end points of the device are $\underline{u}^k$ and $\underline{u}^\ell$, respectively. The relative position of the end points will be denoted $\underline{u}_0 = \underline{u}_0^\ell - \underline{u}_0^k$ and $\underline{u} = \underline{u}^\ell - \underline{u}^k$, in the initial and present configurations, respectively. Note that the rotational degrees of freedom of the structure at the connection points are not involved in this formulation, implying the presence of spherical joints

at these points.

The virtual work done by the hydraulic force is $\delta W = F^h \delta d$, where $\delta d = \delta(\|\underline{u}\| - \|\underline{u}_0\|)$ is a virtual change in device length. This expression then becomes

$$\delta W = F^h \, \frac{\underline{u}^T \delta \underline{u}}{\|\underline{u}\|} = F^h \, \bar{e}^T (\delta \underline{u}^\ell - \delta \underline{u}^k), \qquad (9)$$

where $\bar{e} = \underline{u}/\|\underline{u}\|$ is the unit vector along the axis of the actuator. The forces applied to the external system are

$$\underline{F} = F^h \begin{bmatrix} -\bar{e} \\ \bar{e} \end{bmatrix}, \qquad (10)$$

two forces of equal magnitude and opposite sign applied at the connection points.

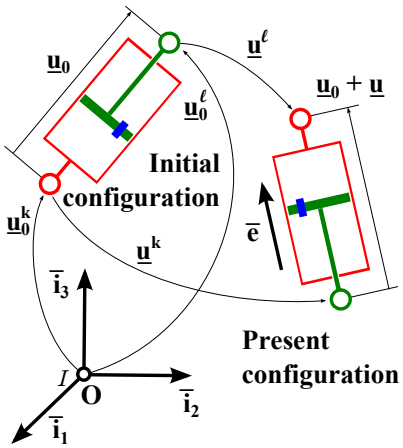

Figure 7: Configuration of the hydraulic device.

4.2 Time discretization of the structural forces

In a typical finite element implementation, the simulation of the system dynamics is discretized in time. The force generated by the hydraulic device will be assumed to remain a constant, F_m^h, over the time step and the work done by this force over the time step now becomes $\Delta W = F_m^h(d_f - d_i)$. This expression is manipulated to become

$$\Delta W = \frac{F_m^h}{2d_m}(d_f^2 - d_i^2) = \frac{F_m^h}{2d_m}(\underline{u}_f^T \underline{u}_f - \underline{u}_i^T \underline{u}_i), \qquad (11)$$

where $d_m = (d_f + d_i)/2$ is the average stroke of the device over the time step. The mid-point relative position vector is defined as $\underline{u}_m = (\underline{u}_f + \underline{u}_i)/2$, and the work expression now becomes

$$\Delta W = F_m^h \, \frac{\underline{u}_m^T}{d_m} \, (\underline{u}_f - \underline{u}_i) = F_m^h \, \underline{e}_m^T \, (\underline{u}_f - \underline{u}_i), \qquad (12)$$

where $\underline{e}_m = \underline{u}_m/d_m$. The discretized hydraulic forces will be selected as

$$\underline{F}_m = F_m^h \begin{bmatrix} -\underline{e}_m \\ \underline{e}_m \end{bmatrix}. \qquad (13)$$

By construction, this discretization guarantees that the work done by the hydraulic force over one time step, eq. (11), is evaluated exactly.

Since the expression for the hydraulic forces and the governing equation of dynamical systems are non-linear, the solution process involves iteration and linearization. Linearization of the discretized forces, eq. (13), leads to

$$\Delta \underline{F}_m = \underline{\underline{K}}_m \begin{bmatrix} \Delta \underline{u}^k \\ \Delta \underline{u}^\ell \end{bmatrix}, \qquad (14)$$

where $\underline{\underline{K}}_m$, the effective stiffness of the actuator, is

$$\underline{\underline{K}}_m = \frac{1}{2} \left\{ \frac{F_m^h}{d_m} \begin{bmatrix} (U - \underline{e}_m \bar{e}_f^T) & -(U - \underline{e}_m \bar{e}_f^T) \\ -(U - \underline{e}_m \bar{e}_f^T) & (U - \underline{e}_m \bar{e}_f^T) \end{bmatrix} + \frac{\mathrm{d}F_m^h}{\mathrm{d}d_m} \begin{bmatrix} \underline{e}_m \bar{e}_f^T & -\underline{e}_m \bar{e}_f^T \\ -\underline{e}_m \bar{e}_f^T & \underline{e}_m \bar{e}_f^T \end{bmatrix} \right\}, \qquad (15)$$

and U is the 3 by 3 identity matrix. This expression requires the evaluation of the derivative of the hydraulic force with respect to the stroke, $\mathrm{d}F_m^h/\mathrm{d}d_m$, that could be computed from the governing equations for the hydraulic device. However, this process is, in general, quite involved. The following approximation was found to be suitable

$$\frac{\mathrm{d}F_m^h}{\mathrm{d}d_m} = \frac{BA_0^2}{V_0} + \frac{BA_1^2}{V_1}; \tag{16}$$

it corresponds to an approximation to the static stiffness of the device.

4.3 Time integration of hydraulic equations

The model described in the previous section requires the knowledge of the hydraulic force acting in the device, given by eq. (8). In turn, this requires the solution of the equations governing the behavior of the hydraulic device, as discussed in earlier sections. Although the model of the hydraulic device is rather simple, a few first order, nonlinear differential equations, it is a numerically stiff set of equations because of the very high "stiffness" of the hydraulic fluid (for typical systems, the bulk modulus of the fluid is about 1.5 GPa). Typically, this problem is overcome by using a very small time step for the integration of the hydraulic equations; for instance, Welsh [3] used a time step of $\Delta t = 10^{-6}$ sec to integrate the equations of a helicopter air-oil strut. While this approach is acceptable when dealing with the sole hydraulic equations, it is not practical to integrate both hydraulic and structural dynamics equations with such a small time step because the computational effort would become overwhelming. Consequently, it is imperative to decouple the integration of the two systems: the structural dynamics equations are integrated with a time step dictated by the frequency content of the structural response, whereas the hydraulic equations are integrated with a much smaller time step.

In this work, the following strategy was used: the structural dynamics equations are integrated with a time step Δt; energy decaying schemes that guarantee nonlinear unconditional stability of the time integration process are used for this purpose, see Refs. [7, 8, 9, 10, 11]. This produces a prediction of the stroking of the hydraulic device, $d_i = \|\underline{u}_i\| - d_0$ and $d_f = \|\underline{u}_f\| - d_0$, the stroking rate has a constant value $\dot{d}_m = (d_f - d_i)/\Delta t$. This information was used to integrate the governing equations of the hydraulic device using a fourth order Runge-Kutta integrator, see Ref. [12]. The time step used in this integrator was $h = \Delta t/N$, *i.e.* N Runge-Kutta steps are performed for each structural time step. Once the hydraulic equations are solved, the pressures in the chambers are predicted and hence the hydraulic device force. The nonlinear solution of the problem is then obtained by iterating between the structural dynamics equations and the hydraulic equations.

5 Numerical Examples

5.1 Hydraulic linear actuator

The first example deals with a hydraulic linear actuator that is used to pitch a beam, as depicted in fig. 8. The system consists of a flexible beam of length $L = 0.8$ m with a 10 kg tip mass connected to a revolute joint at point **R**. At point **C**, located at a distance $d = 0.24$ m from the root of the beam, a flexible horn connects to the beam. Finally, a hydraulic linear actuator is connected between the ground and the tip of the horn at points **S** and **D**, respectively.

The physical properties of the beam and horn are as follows: axial stiffness, 5.7 10^7 N, bending stiffness, 4.275 10^3 N.m^2, shearing stiffness, 1.80 10^7 N, mass per unit span, 2.4 kg/m. The configuration of the hydraulic linear actuator is that depicted in fig. 4. The physical properties of the actuator are listed in Table 1.

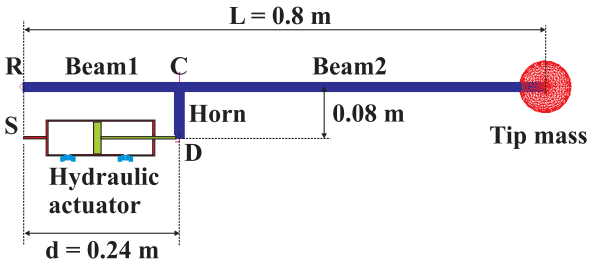

Figure 8: Configuration of the hydraulic linear actuator pitching a beam.

Table 1: Physical properties of the hydraulic actuator.

Quantity	Value
$A_0 = A_1$	7.85 10^{-5} m^2
$V_0 = V_1$	9.42 10^{-6} m^3
$p_{E0} = p_{E1}$	1.25 MPa
$A_{\text{orf0}} = A_{\text{orf1}}$	6.0 10^{-6} m^2
$C_{d0} = C_{d1}$	0.611
p_s	1.0 MPa
B	1.53 MPa

The system was initially at rest. To simulate the actuator's control valves, the throttling areas of both orifices were linearly ramped up from zero to their nominal value in 0.5 s. In the next 0.5 s, the throttling areas were linearly ramped back down to zero. The time step for the structural analysis was set to $\Delta t = 1.0\ 10^{-4}$ s; for each structural step, 48 sub-steps were used for the integration of the hydraulic equations. These time step sizes were selected by a convergence study; it is interesting to note that a large number of sub-steps, 48, was required to achieve the convergence of the integration of the hydraulic equations. The system was simulated for a total period of 1.5 s.

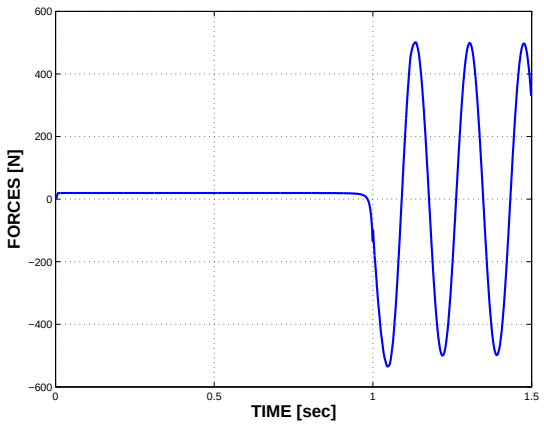

Figure 9: Time history of the force generated by the hydraulic actuator.

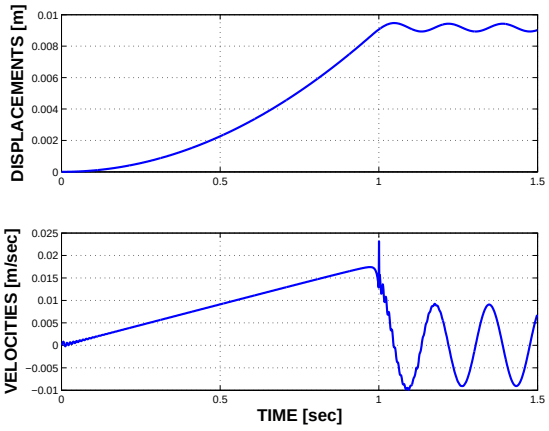

Figure 10: Time histories of the displacement (top figure) and velocity (bottom figure) of the piston of the hydraulic actuator.

Figure 9 shows the time history of the force generated by the hydraulic actuator. Note the nearly constant force generated by the actuator while the throttling areas non zero. Once the throttling areas vanish, the actuator becomes much stiffer. Indeed, the apparent stiffness of the devices is now dictated by the bulk modulus of the oil and it applies much higher forces to the supporting structure. The time histories of the displacement and velocity of the piston of the hydraulic actuator are shown in fig. 10. Once the throttling areas vanish, the length of the actuator remains nearly constant; the

observed oscillations are due to vibrations of the beam-tip mass system following actuation. The interaction between the hydraulic device and the structure is further demonstrated in fig. 11 that shows the time histories of the pressures in the two chambers. Note the sudden drop in chamber 0 pressure at time $t = 1$ s due to the opening of the check valve; the effects of this pressure spike are noticeable on the device velocity and output force, see Figs. 10 and 9, respectively. After the closing of the throttling areas, large variations in chamber pressures are observed resulting from structural vibrations.

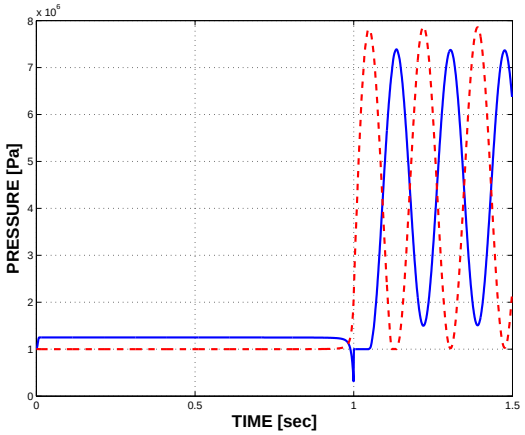

Figure 11: Time histories of the pressures in the two chambers.

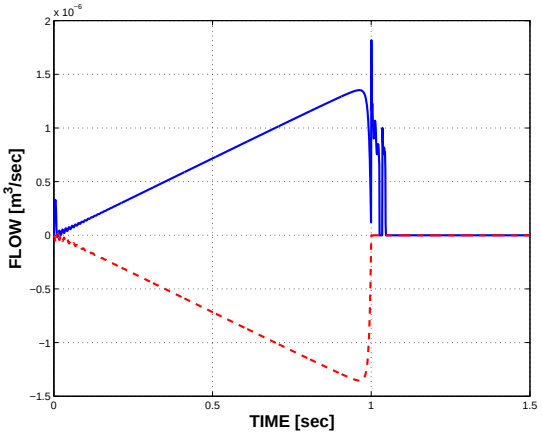

Figure 12: Time histories of the volumetric flow rates into the chamber 0 (solid line) and chamber 1 (dashed line).

Finally, fig. 12 depicts the time histories of the volumetric flow rates into chamber 0 and chamber 1. The flow rates that are observed after the closing of the throttling areas are flow rates through the actuator check valves. The very rapid variations in chamber pressure and orifice flow rates are further evidence of the very high stiffness of the system and help explain the need for the numerous sub time steps required to integrate the hydraulic equations.

5.2 Validation of the model of the UH-60 lead-lag damper

In the next example, a model of the lead-lag damper used in Sikorsky's UH-60 helicopter will be validated by comparing the predictions of the proposed model with measurements taken on a test bench experiment. The physical properties of the hydraulic device are described in reference [3]. The damper was tested under harmonic stroking conditions at a constant circular frequency $\omega = 27.02$ rad/s. Tests were run at various amplitudes of the harmonic motion; fig. 13 shows the experimentally measured peak force in the damper as a function of peak velocity. This figure also shows the predictions of the present model; good agreement is found between measurements and predictions. The time history of the damper force at a peak velocity of 2 in/s is shown in fig. 14 for both model and experiment. While peak loads are in good agreement, force time histories exhibit qualitative differences. First, the experimentally measured force dwells for a short period when it reaches a value near zero; this phenomenon is not predicted by the model and its physical origin is not known; possible explanations are discussed in the next paragraph. Second, the experimental measurements exhibit a different behavior at peak positive and negative forces. This dissymmetry is not present in the model and its physical origin is also unclear.

The following conclusions can be drawn from this calibration effort. The proposed model seems to predict damper peak loads with reasonable accuracy, while the details of the force time history are not predicted to the same level of accuracy. The probable cause of these discrepancies is the highly idealized nature of the present model. Several components of the device, such as the hydraulic

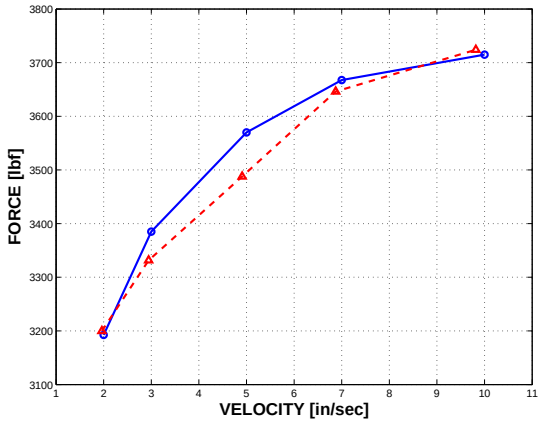

Figure 13: Peak force versus peak velocity. experimental measurements (solid line) and present model predictions (dashedline).

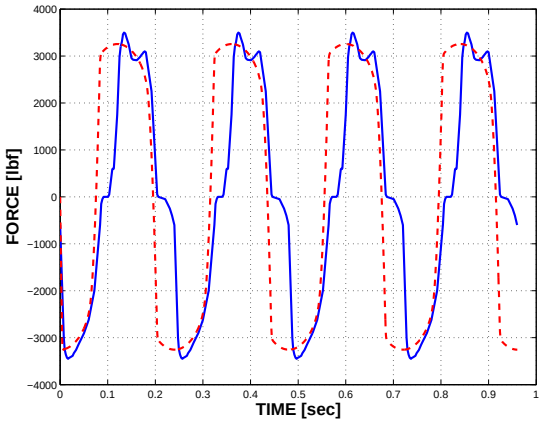

Figure 14: Time history of the lead-lag damper force at a peak velocity of 2 in/s. Experimental measurements: solid line, present predictions: dashed line.

accumulators and check valves, have intrinsic characteristics that have not been modeled in the present effort. Several coefficients of the model, such as the orifice discharge coefficient, have been set to their theoretical values. Other coefficients, such as those appearing in eq. (7), were selected based on indirect, uncertain measurements. Parametric studies performed with the present model have demonstrated the great sensitivity of the predictions to the choice of these coefficients.

5.3 Modeling the UH-60 blade and lead-lag damper

In the final example, the dynamic response of Sikorsky's UH-60 rotor system will be evaluated using a finite element based multibody formulation and a detailed model of the blade hydraulic lead-lag damper. The UH-60 is a four-bladed helicopter whose physical properties are described in Ref. [13] and references therein. In this work, a single blade model will be used. Figure 15 shows the configuration of the rotor system featuring the blade root retention structure, pitch link, pitch horn, swashplate, and lead-lag damper.

The blade was modeled using thirteen cubic beam elements. The root retention structure, from hub to blade, was separated into three segments, having three, two, and two cubic beam elements, respectively, and labeled segment 1, 2 and 3 in fig. 15. The first segment was attached to the rigid hub. The first two segments were connected to each other by an elastomeric bearing modeled by three co-located revolute joints with the following sequence: lag, flap, then pitch rotations. The physical characteristics of the bearing were simulated by springs and dampers in the joints. The next two segments were rigidly connected to each other and to the pitch horn. Finally, the last segment rigidly connected to the blade and damper horn.

The pitch angle of the blade was set by the following control linkages: the swashplate, pitch link, and pitch horn. The pitch link, modeled by three cubic beam elements, was attached to the rigid swashplate by means of a universal joint and to the rigid pitch horn by a spherical joint. The damper arm and damper horn were modeled with rigid bodies. The lead-lag damper was modeled as a hydraulic damper with pressure relief valves, as described in earlier sections; its end points were connected to the damper arm and horn; the physical properties of the device can be found in Ref. [14].

The loads applied to the rotor consisted of the measured aerodynamic loads obtained from in flight test measurements, see ref. [15]. The results presented below correspond to flight counter 8534, a forward flight case with a forward speed of 158 kts. A total of 75 rotor revolutions were

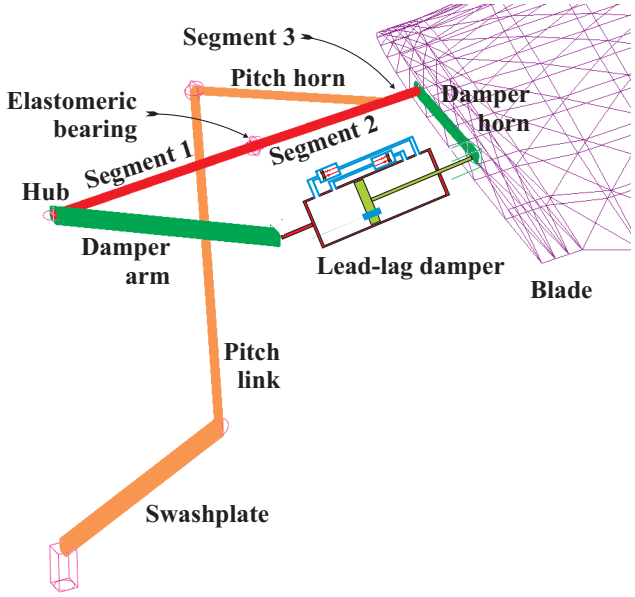

Figure 15: Configuration of Sikorsky's UH-60 rotor system: close-up view of the blade root retention structure, pitch link and pith horn, swashplate, and hydraulic damper.

simulated to allow all transients to die out and obtain a periodic solution. The results presented in the figures below depict the last revolution of the simulation, as a function of the azimuthal angle Ψ. A constant time step size of 256 steps per revolution was used for the structural equations and 25 sub-steps were used for the integration of the hydraulic equations.

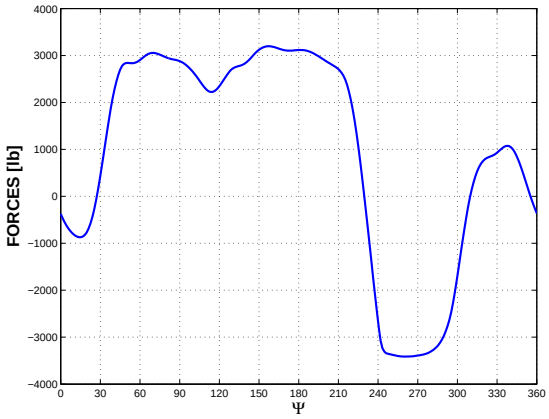

Figure 16: Time history of the lead-lag damper force.

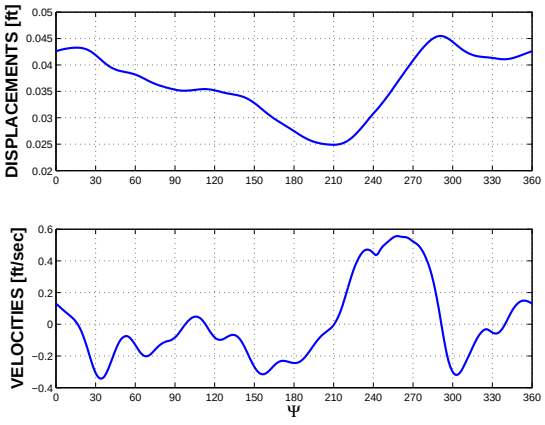

Figure 17: Time history of the lead-lag damper stroking (top figure) and stroking velocity (bottom figure).

Figure 16 displays the time history of the predicted damper force. Note the effectiveness of the pressure relief valves that limit the maximum damping force to about $\pm$ 3200 lbs. The stroke and stroke velocity of the damper are presented in fig. 17. These quantities are the variables forming the basis for empirical models of dampers: the output force is assumed to be a nonlinear function of the instantaneous velocity. In the present model, additional information is available that describes the internal behavior of the device. The pressures in the two chambers of the dampers are shown in fig. 18. Next, the volumetric flow rate through the orifice is shown in fig. 19, this flow rate tends to equilibrate the pressures in the two hydraulic chambers. As expected, the shape of this time history closely follows that of the damper force.

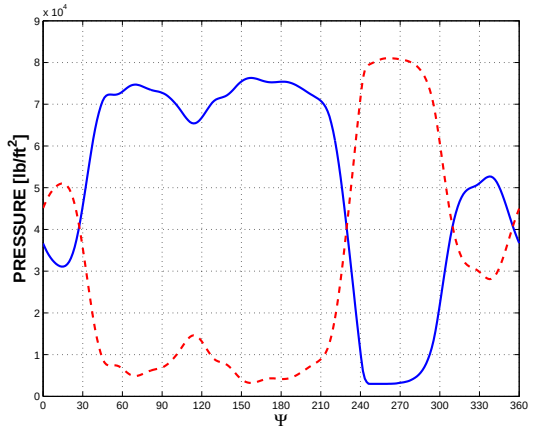

Figure 18: Time history of the predicted pressures in the chamber 0 (solid line) and chamber 1 (dashed line).

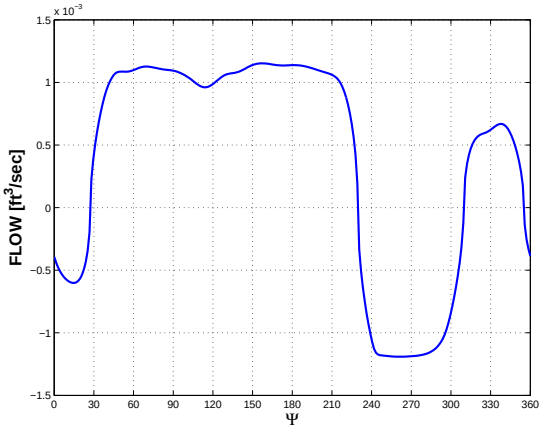

Figure 19: Time history of the predicted volumetric flow rate through the orifice.

The role of the pressure relief valves is illustrated in Figs. 20 and 21 that depict the displacement and velocities of the valves, and the flow rate through these valves, respectively. Valve 0 opens over the azimuthal range $\Psi \in [45, 100]$ then $[125, 215]$ deg, whereas valve 1 opens for $\Psi \in [240, 290]$ deg. These ranges are clearly correlated with the high damper force ranges: positive forces for valve 0, negative forces for valve 1 (see fig. 16). This correlation is also reflected in the hydraulic chamber pressure histories, see fig. 18. When a pressure relief valve opens, the volumetric flow rate through the orifice remains nearly constant, see fig. 19, consistent with the nearly constant pressures in the chambers, see fig. 18. Note that the maximum magnitude of the flow rate through the orifice is of the order of 1.2 10^{-3} ft^3/s, whereas the flow rate through the pressure relief valves, see fig. 21, is nearly an order of magnitude larger, due to larger sectional areas. When open, the pressure relief valve nearly short circuits the two hydraulic chambers, effectively limiting the maximum force output of the device.

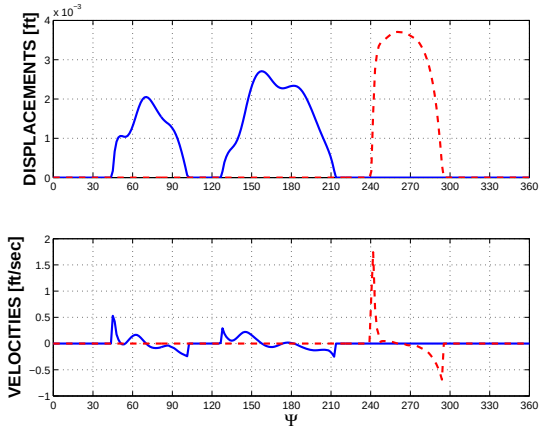

Figure 20: Time history of the predicted displacement (top figure) and velocity (bottom figure) of pressure relief valves. valve 0 (solid line) and valve 1 (dashed line).

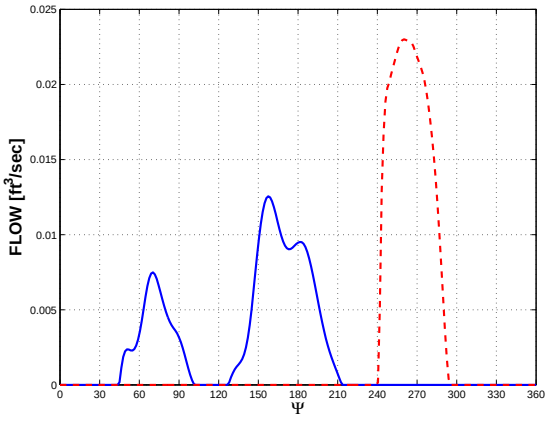

Figure 21: Time history of the predicted volumetric flow rates through the pressure relief valves. valve 0 (solid line) and valve 1 (dashed line).

Finally, fig. 22 shows a comparison between the flight test measurement of damper force and various numerical predictions. In the first simulation, the damper was modeled as a linear dashpot with constant $c = 4659.6$ lb/(ft/s). In the second simulation, a nonlinear dashpot model was used

to represent the damper. The nonlinear dashpot characteristics were obtained from a curve fit of the experimentally measured peak force versus peak velocity relationship given in Ref. [14]. The last simulation uses the proposed model of the hydraulic device. The present model gives a better correlation with the experimental measurements when compared to the simpler models, although discrepancies still exit. Of course, the observed discrepancies are not necessarily a consequence of a lack of accuracy of the damper model. Indeed, the predicted dynamic response of the rotor system involves a complex model with many interacting components; the damper model is but one of these many components.

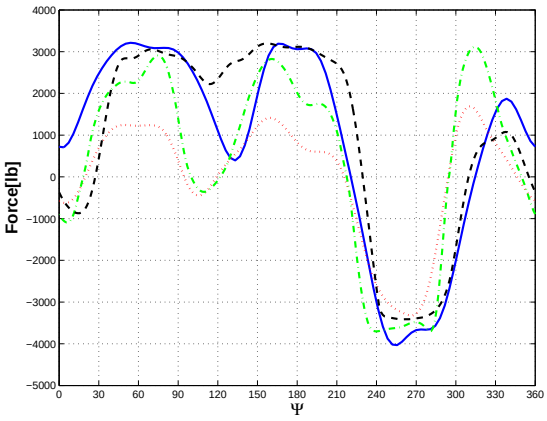

Figure 22: Comparison of the time histories of the lead-lag damper force. Experimental measurements: solid lines; linearized model of the damper: dotted line; nonlinear model of the damper: dashed-dotted line; present model: dashed line.

The probable cause of the observed discrepancy is the cursory nature of the present formulation that models the various components of hydraulic devices with simple equations involving empirical parameters. Some model parameters were set to their theoretical values; others were not known with sufficient accuracy in the experimental set-up, in particular, the hydraulic circuit pressure or the relief valve sectional area. The physical behavior of several components of the device, such as the hydraulic accumulators and check valves, were highly idealized. Other physical phenomena, such as friction in the damper, are not presently modeled and are difficult to quantify with the available experimental data.

This discussion clearly points to the need for more detailed experimental studies of hydraulic devices. Systematic bench test experiments with detailed measurements of chamber pressures, relief valve positions, check valves positions and their associated flow rates or velocities would provide the needed experimental basis for the validation of advanced models.

6 Conclusions

1. A methodology allowing physics based modeling of hydraulic devices within multibody-based comprehensive models of rotorcraft systems was developed.

2. The new mathematical models of hydraulic devices were implemented in a multibody code and calibrated by comparing their predictions with bench test measurements. While predicted peak damping forces were found to be in good agreement with measurements, the model did not predict the entire time history of damper force to the same level of accuracy.

3. The validated model of the UH-60 lead-lag damper model was coupled with a comprehensive model of the rotor system. Measured aerodynamic loads were applied to the blade and

predicted damper forces were compared with experimental measurements. A marked improvement in the prediction was observed when using the proposed model rather than a linear approximation of the damper behavior.

4. The proposed model also evaluates relevant hydraulic quantities such as chamber pressures, orifice flow rates, and pressure relief valve displacements. Hence, the present model could be used to design lead-lag dampers presenting desirable force and damping characteristics.

7 Acknowledgements

This work was sponsored by the National Rotorcraft Technology Center and the Rotorcraft Industry Technology Association under contract WBS No. 2003-B-01-01.1-A1; Dr. Yung Yu is the contract monitor.

References

[1] T.J. Viersma. *Analysis, Synthesis and Design of Hydraulic Servo-Systems and Pipelines*. Elsevier, Amsterdam, 1980.

[2] R.H. Canon. *Dynamics of Physical Systems*. McGraw-Hill Book Company, New York, 1967.

[3] W.A. Welsh. Simulation and correlation of a helicopter air-oil strut dynamic response. In *American Helicopter Society 43rd Annual Forum Proceedings*, St. Louis, Missouri, May 18-20 1987.

[4] W.A. Welsh. Dynamic modeling of a helicopter lubrication system. In *American Helicopter Society 44th Annual Forum Proceedings*, Washington, DC, June 16-18 1988.

[5] O.A. Bauchau, C.L. Bottasso, and Y.G. Nikishkov. Modeling rotorcraft dynamics with finite element multibody procedures. *Mathematical and Computer Modeling*, 33(10-11):1113–1137, 2001.

[6] A. Cardona and M. Géradin. Modeling of a hydraulic actuator in flexible machine dynamics simulation. *Mechanisms and Machine Theory*, 25(2):193–207, 1990.

[7] O.A. Bauchau and N.J. Theron. Energy decaying scheme for non-linear beam models. *Computer Methods in Applied Mechanics and Engineering*, 134(1-2):37–56, 1996.

[8] O.A. Bauchau and N.J. Theron. Energy decaying schemes for nonlinear elastic multi-body systems. *Computers & Structures*, 59(2):317–331, 1996.

[9] O.A. Bauchau. Computational schemes for flexible, nonlinear multi-body systems. *Multibody System Dynamics*, 2(2):169–225, 1998.

[10] O.A. Bauchau and C.L. Bottasso. On the design of energy preserving and decaying schemes for flexible, nonlinear multi-body systems. *Computer Methods in Applied Mechanics and Engineering*, 169(1-2):61–79, 1999.

[11] O.A. Bauchau, C.L. Bottasso, and L. Trainelli. Robust integration schemes for flexible multibody systems. *Computer Methods in Applied Mechanics and Engineering*, 192(3-4):395–420, 2003.

[12] W.H. Press, B.P. Flannery, S.A. Teutolsky, and W.T. Vetterling. *Numerical Recipes. The Art of Scientific Computing*. Cambridge University Press, Cambridge, 1990.

[13] W.G. Bousman and T. Maier. An investigation of helicopter rotor blade flap vibratory loads. In *American Helicopter Society 48th Annual Forum Proceedings*, pages 977–999, Washington, D.C., June 3-5 1992.

[14] J. J. Howlett. Uh-60a black hawk engineering simulation program: Vol. i - mathematical model. Technical report, NASA CR-166309, December 1981.

[15] R.M. Kufeld, D.L. Balough, J.L. Cross, K.F. Studebaker, C.D. Jennison, and W.G. Bousman. Flight testing of the UH-60A aircraft. In *American Helicopter Society 50th Annual Forum Proceedings*, Alexandria, VA, May 11-13 1994.